Spectral and spatial shaping of Smith-Purcell radiation

Roei Remez, Niv Shapira, Charles Roques-Carmes, Romain Tirole, Yi Yang, Yossi Lereah,

Marin Soljačić, Ido Kaminer, and Ady Arie

Spectral and spatial shaping of Smith Purcell radiation

Roei Remez[1]*, Niv Shapira[1], Charles Roques-Carmes[2], Romain Tirole[2,3], Yi Yang[2],
Yossi Lereah[1], Marin Soljačić[2], Ido Kaminer[2,4] and Ady Arie[1]
[1]School of Electrical Engineering, Fleischman Faculty of Engineering, Tel Aviv
University, Tel Aviv, Israel.
[2]Research Lab of Electronics, MIT, Cambridge, MA 02139, USA
[3]Department of Physics, Faculty of Natural Sciences, Imperial College London,
London SW7 2AZ, UK
[4]Department of Electrical Engineering, Technion – Israel Institute of Technology,
Haifa 32000, Israel
*Correspondence to: roei.remez@gmail.com.

Abstract
The Smith Purcell effect, observed when an electron beam passes in the vicinity of a
periodic structure, is a promising platform for the generation of electromagnetic
radiation in previously-unreachable spectral ranges. However, most of the studies of
this radiation were performed on simple periodic gratings, whose radiation spectrum
exhibits a single peak and its higher harmonics predicted by a well-established
dispersion relation. Here, we propose a method to shape the spatial and spectral far-
field distribution of the radiation using complex periodic and aperiodic gratings. We
show, theoretically and experimentally, that engineering multiple peak spectra with
controlled widths located at desired wavelengths is achievable using Smith-Purcell
radiation. Our method opens the way to free-electron driven sources with tailored
angular and spectral response, and gives rise to focusing functionality for spectral
ranges where lenses are unavailable or inefficient.

A. Introduction

Ever since its first observation in 1953 [1], Smith Purcell Radiation (SPR) has been
studied extensively, mainly due to its potential to generate light at hard-to-reach
electromagnetic frequencies, such as the far-infrared, terahertz, and x-ray ranges [2–
7]. This radiation, which originates from the collective oscillations of charges induced
by free charged particles above a periodically patterned surface, is characterized by a
specific dispersion relation and emission at every angle in the plane normal to the
surface.

The community has explored various theories to account for the physics of this
phenomenon in metallic gratings [8–11] and to increase the efficiency of the
radiation [5,6,12,13]. Even more advanced theories revealing quantum features of this
effect [14,15] assumed simple periodic structures, giving a momentum $n\frac{2\pi}{\Lambda}\vec{x}$ to the
incoming electron (where n and Λ are the diffraction order and grating period,
respectively). Recently, the study of SPR was extended beyond the simple periodic
structure, into aperiodic arrays [16], disordered plasmonic arrays [17], and Babinet
metasurfaces for manipulating the SPR polarization [18]. However, to the best of our
knowledge, no attempt has been made to shape the angular spectrum and frequency
spectrum of SPR.

In this Paper, we develop a systematic method for shaping the SPR's angular and
frequency spectrum using complex periodic and aperiodic gratings. First, we show
theoretically and experimentally that the single peak of the conventional SPR far-field
distribution can be split into a desired set of peaks by properly designing a complex
periodic grating, and demonstrate twin-peak and triple-peak shaping. We then discuss

the advantages and limitations of the method and study the effect of the interaction length on the radiation, showing that it can be used to smoothen the spectral or angular response for a desired outcome. We conclude with a theoretical suggestion corroborated by a set of simulations for a Smith-Purcell cylindrical lens.

B. A theoretical analysis of Smith-Purcell radiation in complex periodic gratings

We start with writing the expression of the field emitted from an infinite metallic periodic grating, positioned at (x, y) plane with the rulings parallel to the y direction, and where the electron is passing close to the grating with velocity $v_0\hat{x}$, as proposed by Van Den Berg [8]:

$$E_x(x,y,z,t) = \frac{1}{2\pi^2} Re\left[\int_0^\infty d\omega \int_{-\infty}^\infty d\beta \sum_{n=-\infty}^\infty \epsilon_{xn}^r(\beta,\omega)e^{i\alpha_n x+i\beta y+i\gamma_n z-i\omega t}\right] \quad (1)$$

where $\alpha_n = \frac{\omega}{v_0} + \frac{2\pi n}{\Lambda} = k_0\sin\phi\sin\theta_n$, $\beta = k_0\cos\phi$, $\gamma_n = \sqrt{k_0^2 - \beta^2 - \alpha_n^2}, k_0 = \frac{\omega}{c} = \frac{2\pi}{\lambda_0}, \lambda_0$ and ω are the vacuum wavelength of light and its angular frequency, c is the velocity of light, ϕ is the angle of the wave vector with y axis and θ_n is the angle of the projected k vector on the (x, z) plane with z axis (see Fig. 1). The discrete summation over n originates from the different diffraction orders of the grating, with corresponding spatial frequency components α_n and γ_n. Although the summation is on all values of n, we note that for high diffraction orders γ_n becomes imaginary and the wave is therefore evanescent. From the equation for α_n we can formulate the dispersion equation:

$$\lambda_0 = \frac{\Lambda}{n}\left(\sin\phi\sin\theta_n - \frac{c}{v_0}\right) \quad (2)$$

Which is equivalent to the dispersion relation from the first paper by Smith and Purcell [1]. Eq. (1) represents decomposition into plane waves in direction (θ_n, ϕ). Defining E_{xn} as the complex electric field of the nth diffraction order,
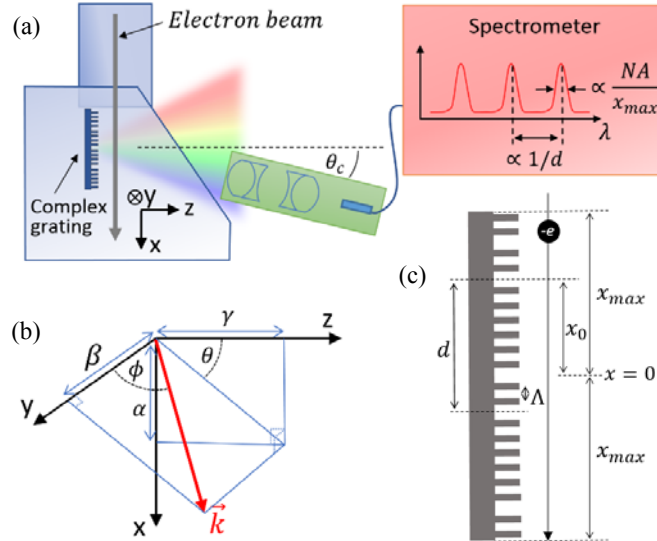

Figure 1 – Experimental setup. (a) The special grating was positioned inside the viewing chamber of the transmission electron microscope, while the output radiation is collected using lenses and a spectrometer located outside the microscope. Inset to (a) – the spectral response of the first diffraction order of the radiation exhibit multiple peaks with spacing and width inversely proportional to the dislocation period and the interaction length, respectively. (b) – Definition of angles and momentum components of the emitted light. ϕ is the angle between the wave-vector of the emitted light and the y axis, and θ is the angle between the projection of the $\vec{k}$ vector on the xz plane and the z axis. (c) Schematic drawing of a complex periodic grating, showing the supercell of period d created by half-period spacings on an otherwise constant period Λ.

$$E_{xn} = \frac{1}{2\pi^2} \int_0^\infty d\omega \int_{-\infty}^\infty d\beta \, \epsilon_{xn}^r(\beta, \omega) e^{i\alpha_n x + i\beta y + i\gamma_n z - i\omega t},$$

we can approximate the electric field emitted in the case of a structured grating (SG) as:

$$E_x^{SG}(x, y, 0, t) = \text{rect}\left(\frac{x - x_0}{2x_{max}}\right) \sum_{n=-\infty}^\infty f_n(x) E_{xn}(x, y, 0, t) \quad (3)$$

Where $2x_{max}$ is the interaction length of the electron with the grating, x_0 is the center of the interaction with respect to an arbitrary point at the grating, and $f_n(x)$ denotes the effect of the deviation from a periodic grating on the electric field of the nth diffraction order at the grating's plane z=0. We note that in a single SPR experiment, usually many values of x_0 are measured simultaneously, since the non-zero width of the electron beam gives different interaction area for each electron.

To exemplify our method, we limit our derivation for the case of constant duty cycle (ridge to period ratio) of 50%, which results with phase-only changes for the electric field at $z = 0$. We can define a function $s(x)$ that expresses the structuring of the grating (the results below can be directly generalized to any duty cycle and even arbitrary grating shapes). A shift of $s(x)\Lambda$ in the grooves position (where $0 \leq s(x) \leq 1$) will result in phase shift $\Delta\psi_n$ for order n of the electric field at z=0, given by $\Delta\psi_n = 2\pi s(x)n$, where n is the SPR diffraction order (See [19] for Huygens construction of this expression). Therefore, $f_n(x) = e^{i2\pi s(x)n}$. Here, the function $s(x)$ (and therefore $f_n(x)$) is assumed periodic of period d, however as we discuss in section D this does not have to be the case, and some interesting results can be achieved with non-periodic variations of the grating. The electric field at the grating plane can be rewritten as a far-field expression, defining the far-field angular distribution $\eta_x^r(\alpha, \beta, \omega)$:

$$E_x^{PG}(x, y, 0, t) \equiv \frac{1}{2\pi^2} \int_0^\infty d\omega \int_{-\infty}^\infty d\beta \int_{-\infty}^\infty d\alpha \, \eta_x^r(\alpha, \beta, \omega) e^{i\alpha x + i\beta y - i\omega t} \quad (4)$$

Comparing Eq. (3) and (4), we get

$$\eta_x^r(\alpha, \beta, \omega) = 2x_{max} \sum_{n=-\infty}^\infty e^{-i\alpha x_0} \epsilon_{xn}^r(\beta, \omega) \, \text{sinc}((\alpha - \alpha_n(\omega))x_{max}) \otimes \text{FT}\{f_n(x)\}$$

Where $\text{FT}\{f_n(x)\}$ is the Fourier transform of $f_n(x)$, and $\otimes$ denotes convolution. Since $f_n(x)$ is periodic, we can write its Fourier transform as a Fourier series $\text{FT}\{f_n(x)\} = \sum_{m=-\infty}^\infty a_{mn}\delta\left(\alpha - \frac{2\pi m}{d}\right)$, where d is the period of $f_n(x)$ and a_{mn} are Fourier coefficients:

$$a_{mn} = \frac{1}{d} \int_d e^{i2\pi s(x)n} e^{i2\pi mx/d} dx \quad (5)$$

Finally, the angular far-field expression is given by:

$$\eta_x^r(\alpha, \beta, \omega) = 2x_{max} \sum_n \epsilon_{xn}^r(\beta, \omega) \sum_m a_{mn} e^{-i\left(\alpha - \frac{2\pi m}{d}\right)x_0} \text{sinc}\left(\left(\alpha - \frac{2\pi m}{d} - \alpha_n\right)x_{max}\right) \quad (6)$$

where $2x_{max}$ is the interaction length of the electron with the grating, x_0 is the position of the interaction area with respect to an arbitrary point in the grating, and are the phase Fourier coefficients [19]. If the optical collecting system has a finite aperture ξ, centered around angular coordinates $(\theta, \phi) = (\theta_c, \pi/2)$, the measured power for each angular frequency ω will be proportional to the integration of the intensity of that frequency over the collecting aperture:

$$P(\omega) \propto \iint_{\xi} |\eta_x^r(\alpha, \beta, \omega)|^2 \, d\alpha \, d\beta \qquad (7)$$

For small collecting aperture with angular diameter $A < \frac{2\pi}{dk_0}$ and interaction length larger than the period of the variation, $2x_{\max} > d$, Eq. (6) and (7) give a spectrum with a series of separated peaks. The peaks are centered at wavelengths λ_{mn} yielding (for $\phi = \pi/2$):

$$\lambda_{mn} = \frac{sin\theta_c - \frac{c}{v_0}}{\frac{n}{\Lambda} + \frac{m}{d}} \qquad (8)$$

The expression is identical to the ordinary SPR equation (Eq. (2)) for the zero-th order $m=0$, but for $m \neq 0$, additional peaks appear in different locations which are determined by the variation periodicity d. Interestingly, the zero-th order amplitude a_{0n} can be canceled, eliminating the original SPR peak, by adequately designing the structuring function $s(x)$ so the phase $e^{i\Delta\psi}$ averages to zero (as in Fig. 2). The width of the peaks is set by the interaction length $2x_{\max}$ and by the aperture of the collection system. Increasing the aperture A, or decreasing the interaction length $2x_{\max}$ (as in Fig. 3) widens the spectral peaks while their central wavelength remains constant, until the peaks become inseparable. Since it is assumed that each electron has a different value of x_0, the radiation from different electrons is summed incoherently with equal distribution of x_0 between 0 and d.

C. Spectral shaping of SPR

Fig. 2 demonstrates the modification of the first diffraction order (n=-1) of SPR using structures with a half-period shift every M/2 periods of the grating, therefore $d = (M + 1)\Lambda$. For example, see Fig. 2(a) for schematic grating illustration when M=16 ($\Lambda = 400nm$ for all gratings). The phase of the emitted light is zero for M/2 periods, then π for M/2 periods, then zero again for M/2 periods and so on. Therefore, the emitted light has a phase periodicity of (M+1) periods, when the +1 is needed because of the two half-period shifts. In this case, the two dominant Fourier coefficients in Eq. (5) are a_1 and a_{-1}, as shown in Fig. 2(b), where we have omitted the n subscript $a_m \equiv a_{m,n=-1}$. Importantly, this nulls the zero-the order Fourier coefficient a_0, which defines the amplitude of the original SPR diffraction expression (Eq. (2)). For these type of $s(x)$ functions we therefore expect the original SPR spectral peak of the $n = -1$ order to be zero.

The gratings for the experiments in this Paper were fabricated using electron-beam lithography on a 500 micron BK7 substrate, coated with 200nm silver, and resulting with grooves height of another 190nm of silver and about 50% duty cycle. The gratings were placed inside the viewing chamber of an FEI-Technai 200KeV electron microscope, and were aligned to be almost parallel to the electron beam. The optical setup outside the microscope's viewing chamber consisted of two 2" doublet lenses, chromatically corrected for the measured spectral range, and a collecting fiber, connected to an Avantes ULS2048L spectrometer with a spectral resolution of 1.4 nm (See Fig. 1(a)). A circular aperture of 13mm, placed 27cm from the grating, was used to limit the angular acceptance of the light collection system in all the experiments in this Paper, therefore the full acceptance angle was 48 mrad.

The experimental and theoretical spectral responses for different M values are given in Fig. 2(c-e). The twin-peak spectral shape is clearly visible for M = 16 (Fig. 2c).

When M increases, the two peaks get closer to one another, until for M = 64 (Fig. 2e) they are no longer separated, because of the limited interaction distance that depicts the number of unit cells (~30) that the electron is interacting with. By optimizing the first of the measured width to simulation, we estimate the value for the interaction length to be 12 microns. Using this value alone, our theory shows a very good fit to all spectra (red curves in Figs. 2(c-e)). Figs. 2(c-e) where taken for the same value of θ_c which we measure to be $-7.7 \pm 1.5 \ deg$, close to -8.2 deg that optimizes the fit of theory and experiments.

Fig. 2(f-h) presents the same grating of Fig. 2(d) for different collecting angle θ_c, showing that the main effect of changing the angle of collection is the wavelength
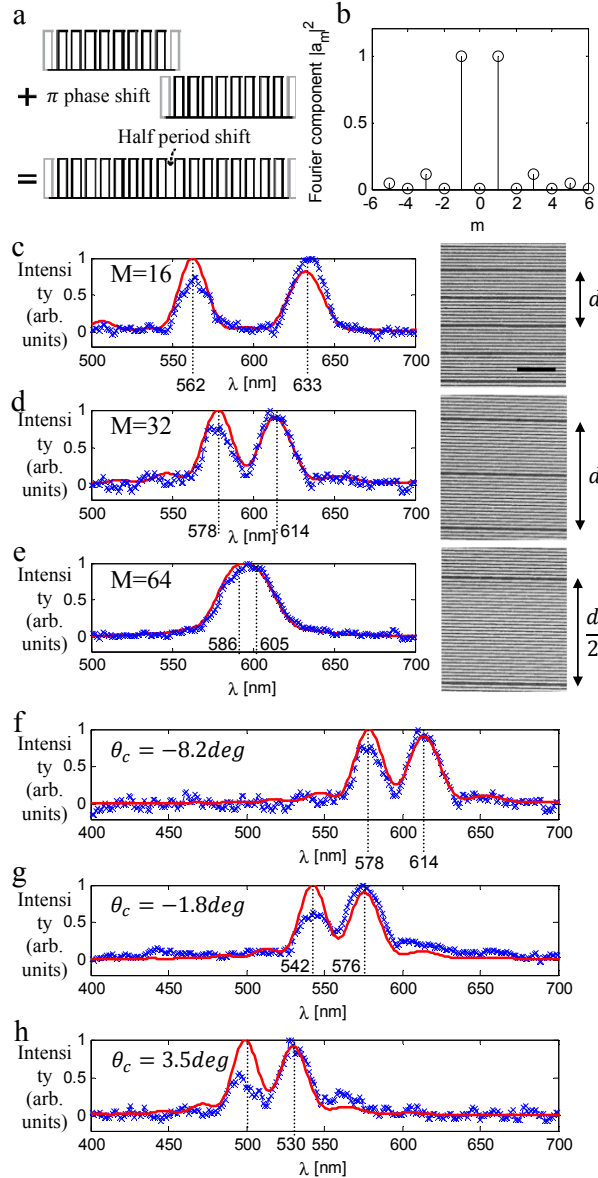

Figure 2 – Spectral splitting of Smith-Purcell peak. (a) Schematic demonstration of half-period shift. (b) The Fourier components of the phase function, showing two main peaks of the ±1 orders and a suppressed zero order. (c-h) Theoretical (according to Eq. (7), solid red) and experimental (blue x's) Smith Purcell radiation spectrum for twin peak designs. Marked: peak locations according to Eq. (8), for $m = \pm 1$. (c-e) Spectral response for $\theta_c = -8.2 \ deg$, for different M values. Λ =400 nm for all three gratings. Insets to (a-c) – Scanning Electron Microscope images of the gratings used for (c-h), scale bar is 5 microns. (f-h) Spectral response for the grating of M=32, for different θ_c values.

translation of the response, much like in regular SPR. Therefore, the far-field distribution of a single wavelength also maintains a twin-peak angular distribution. We note that the difference between the theoretical and the experimental curves is the result of the assumption that $\epsilon_{xn}^r(\beta, \omega)$ is constant for different light frequencies. The presented optimized values of θ_c: -8.2 -1.8 and 3.5 degrees for Fig 2(f-h), are well inside the error range (± 1.5 degrees) of the measured values: -7.7, -1.2 and 2.2 degrees respectively.

Efficient SPR emission by the electrons is only possible when the electron passes in proximity to the grating surface within the interaction range ($z < h_{int}$). The ω component of the electrostatic field of an electron of velocity v decays transversely within a range [3,9]: $h_{int} \approx \tilde{\beta}\tilde{\gamma}\lambda/4\pi$, where $\tilde{\beta} = v_0/c$ and $\tilde{\gamma} = \left(1 - \tilde{\beta}^2\right)^{-0.5}$. In our case $\tilde{\beta} = 0.7$, and for small θ values ($\lambda \approx \frac{\Lambda}{\tilde{\beta}} = 0.57\mu m$) this corresponds to $h_{int} \approx 45\ nm$. We note that the estimation of h_{int} is used later only to approximate the experimental beam alignment capabilities, as we concentrate on shaping the emitted radiation rather than predicting the radiation energy.

The finite interaction length limits our spectral control as is apparent from Fig. 2e, where the two peaks merge into a single wider peak. The limited interaction length in our experiments is the result of the angle between the electron beam and the grating,
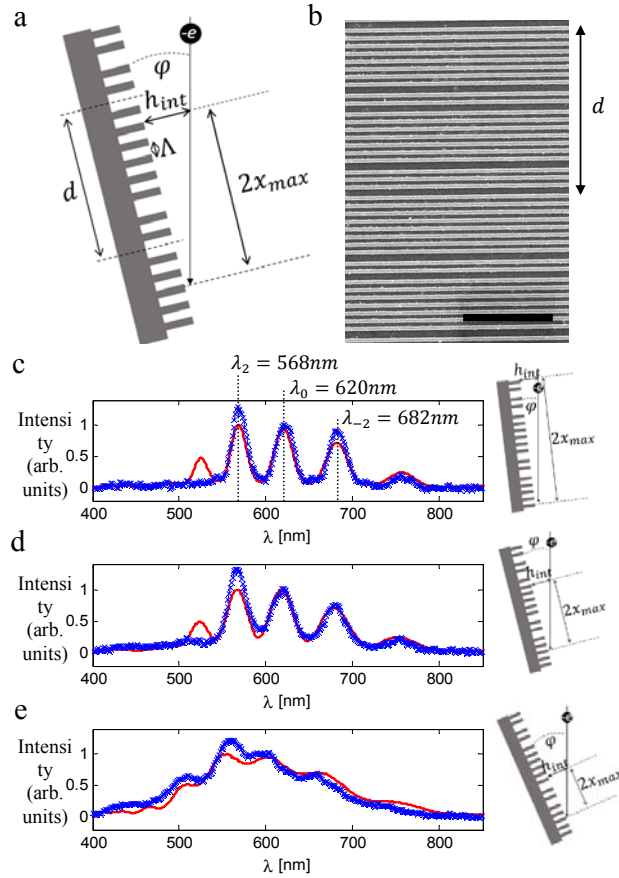

Figure 3 – Influence of the interaction length on spectral shaping. (a) – Schematic drawing showing the change of interaction length caused by varying the angle between the electron beam and the grating. (b) – Scanning Electron Microscope Image of grating for 5 peak design. Scale is 5 micron. (c-f) - Theoretical (according to Eq. (7) , solid red) and experimental (blue x's) Smith Purcell radiation spectrum for three-peak design, for different interaction lengths, changed by altering the angle between the electron beam and the grating. Marked: wavelengths $\lambda_m = \lambda_{m,n=-1}$ according to Eq. (8).

marked as φ in Fig. 3(a). Ideally, this angle would be zero, however the width of the electron beam and alignment limitations in our setup prevent us from achieving perfect parallelism. Interestingly, we can also use this angle degree of freedom to our advantage when a wider-spectrum source is desired: increasing φ causes the peaks to widen and creates a smoother spectrum due to smaller interaction length. To investigate this further we use a grating design (Fig. 3(b)) that exhibits triple-peak response (the -2, 0 and +2 Fourier coefficients; see [19] for the design of this grating). Fig. 3(c) presents the measured spectrum using the same aperture and Λ values as the previous experiment, along with a theoretical curve to which the interaction length was fitted to be $10\ \mu m$ (or 25Λ). Beam angle or beam angular spread of about $5\ mrad$ can cause such a coherence length limit, considering the estimated value of $h_{int} = 45\ nm$. Deliberately increasing the angle φ between the electron beam and the grating decreases the interaction length and widens the spectral peaks (Figs. 3(d,e)). This confirms the interpretation of SPR as a coherent diffraction effect to which each unit cell is contributing. Note that the collection angle θ_c is effectively shifted by φ (even when the collection system in the lab remains fixed). The values after optimization for Fig. 3(c), (d) and (f) were $\theta_c = -7, -6.7,$ and -4.8 deg, while $2x_{max} = 10, 7,$ and 4.6 micron, respectively.

D. Spatial shaping of SPR

The concepts we outlined above further enable to investigate ways to shape the spatial response of SPR. For instance, we propose here a general design for a "Smith Purcell lens" that will focus the emitted radiation at a predesigned point in (x, z) plane. This way the SPR source will multiplex the functionality of the source and the lens, which for certain spectral ranges (e.g., extreme ultraviolet) may be inefficient or nonexistent. A lens designed for wavelength λ_c ($k_c = 2\pi/\lambda_c$) with focal length f_{len}, focused to an off-axis point with angle ζ with z axis, as illustrated in Fig. 4, requires a phase modulation of the form

$$\Delta\psi = k_c\sqrt{f_{len}^2 - x^2} + k_c x \sin\zeta$$

Therefore, the angle of the emitted radiation from point x on the grating should be $sin\theta_n = \frac{1}{k_c}\frac{d(\Delta\psi)}{dx}$. From Eq. (2) we get (for $\phi = \pi/2$):

$$\Lambda(\text{x}) = \frac{n\lambda_c}{\dfrac{x}{\sqrt{f_{len}^2 - x^2}} + \sin\zeta - \dfrac{c}{v_0}} \approx \frac{n\lambda_c}{\dfrac{x}{f_{len}} + \sin\zeta - \dfrac{c}{v_0}}$$

This result can also be explained using the shift function $s(x)$ notation, as we show in the Supplemental Material [19]. We note that the convergence exists only at x-z plane, and the divergence at the y-z plane is left unchanged. Therefore, this device functions as a cylindrical lens to the emitted radiation.

In order to further explore this device, we used time-domain simulations using the commercial FDTD software Lumerical. The electron beam can be represented as a time-dependent propagating point-electron: $J(\vec{r}, t) = -e\ v\ \delta(x - vt)\delta(y - y_0)\delta(z - z_0)$, and the associated polarization is $P(\vec{r}, \omega) = i\frac{e}{\omega}\exp(-i\frac{\omega x}{v})\ \delta(y - y_0)\delta(z - z_0)\ \vec{x}$. We model the electron beam by a set of closely spaced dipole sources, in order to induce a polarization similar to $P(\vec{r}, \omega)$. As can be seen in Fig. 4(c), a chirped grating focuses the emitted radiation for wavelength λ_C. If another

wavelength $\tilde{\lambda}$ is used other than the design wavelength λ_c, we'll get (for $x \ll f_{len}$ and
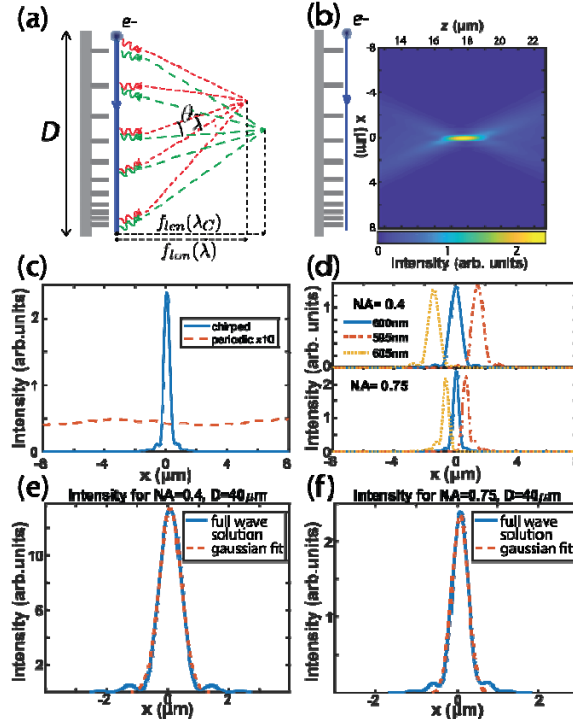

Figure 4 - Spatial shaping of SPR: design of a Smith-Purcell lens. (a) Schematic description of Smith-Purcell "cylindrical lens", designed to focus a wavelength λ_c at focal distance $f_{len}(\lambda_c)$ and suffering chromatic aberration for other wavelengths. (b) Far-field radiation full-wave simulation as a function of the distance from the chirped grating. The length of the surface is D=40µm (giving NA=0.75), the acceleration voltage is 20keV and the focused wavelength λ_C = 600nm. (c) Comparison chirped-grating far-field radiation in the focal plane, with a grating of constant period Λ=163nm (same as the average period of the chirped grating, the intensity being multiplied by 10 to appear on the same scale). (d) Far-field radiation of multiple wavelengths in the focal plane with NA = 0.4 (top), NA = 0.75 (bottom). (e,f) - Intensity profile in the focal plane for (e) NA = 0.4 and (f) NA = 0.75. In (e) (resp. (f)), the measured FWHM (using Gaussian fit) is 855nm (resp. 470nm), compared to a diffraction-limited performance of 750nm (resp. 400nm).

$\zeta = 0$):

$$sin\theta = \frac{\tilde{\lambda}n}{\Lambda(x)} + \frac{c}{v_0} = \frac{x}{\frac{\lambda_c}{\tilde{\lambda}}f_{len}} + \left(1 - \frac{\tilde{\lambda}}{\lambda_c}\right)\frac{c}{v_0}$$

Therefore, wavelength $\tilde{\lambda}$ will have a different focal length, given by $\tilde{f}_{len} = \frac{\lambda_c}{\tilde{\lambda}}f_{len}$. The rightmost term is the tilt expected for wavelength $\tilde{\lambda}$ at x=0, and gives the angle $\theta_{\tilde{\lambda}}$ between the center of the converging cone of each wavelength, $sin\theta_{\tilde{\lambda}} = \left(1 - \frac{\tilde{\lambda}}{\lambda_c}\right)\frac{c}{v_0}$. This spectral behavior is demonstrated in Fig. 4(a,d). We observe in our simulations (Fig 4(e,f)) a focusing performance of 11.4% (resp. 17.5%) above diffraction limit for NA = 0.4 (resp. NA = 0.75). See [19] for further spectral and diffraction analysis of such lens.

We conclude that this cylindrical-lens-like device has strong axial chromatic dispersion, and the expected lateral chromatic dispersion of ordinary SPR. The high chromaticity of this device would be of interest for applications were a small bandwidth is required (deep UV lithography, mask inspection, and biological applications [20–22]) and spectrometry. Even though there has not been, to the best of our knowledge, any experimental demonstration of Smith-Purcell radiation in the

deep ultraviolet so far, there are promising theoretical predictions in the literature [23,24], paving the way to an efficient, tunable source in the ultraviolet.

The highly dispersive nature of a Smith-Purcell lens shown in Fig. 4(d) would make the experimental demonstration of its close-to-diffraction-limited behavior challenging, at least with conventional broadband imaging systems (for instance, CCD cameras). This limitation could be circumvented by designing chirped metasurfaces made of resonators with a very high spectral quality factor or plasmon-locked SPR as has been recently proposed [25]. The latter approach relies on phase-matching the plasmon dispersion relation with the electron beam line $\omega = kv$, thus preventing applications to extreme UV regimes. Other dispersion engineering tricks should also be investigated from, for instance, the field of achromatic metasurfaces [26].

E. Conclusions

In this Paper, we have demonstrated how Smith-Purcell radiation can be shaped to a desired spectral or angular far-field response. Its resolution is limited only by the interaction length of the electrons with the modified grating. By carefully engineering the grating modulation function $s(x)$, and the resulting Fourier components a_{nm} from Eq. (5), it is possible to create a light source with arbitrary spectral and angular shape, at spectral ranges that are unreachable with conventional light sources. While most research in this field so far dealt with simple periodic gratings, for which the spectral and angular response have a single peak (whose location is given by the ordinary Smith Purcell dispersion Eq. (2) [1]), our method enables shaping the radiation spectrum into arbitrary line-shapes, exemplified by our measured dual- and triple-peaked spectra. Furthermore, the method is not limited to periodic phase manipulations, and as we suggested one can use it to create a lens for a specific emitted wavelength, converging the beam in x-z plane. This might be useful for spectral ranges where lenses are hard to achieve, such as the UV or x-ray ranges [7].

We note that although the interaction length seems to impose a limitation on the widths of the peaks, the concept of super-oscillations [27,28] might be used together with our method to achieve peaks at arbitrary small widths (with penalty to the emitted intensity). The concepts of holography [29] can be used to design the structuring function $s(x)$ for shaping the complex Smith-Purcell emitted waveform (as was already demonstrated for transition radiation [30]). This can be achieved for example by varying other parameters of the grating structure such as the duty cycle, the ridge height, or the profile shape of the periods. Furthermore, in our theoretical analysis the value of $\epsilon_{xn}^r(\beta, \omega)$ is assumed constant, which explains the deviation of the peaks height from the theoretical curves. Therefore, this approach might be used to measure the function $\epsilon_{xn}^r(\beta, \omega)$ at a single spectral measurement.

References

1. S. J. Smith and E. M. Purcell, "Visible Light from Localized Surface Charges Moving across a Grating," Phys. Rev. **92**, 1069–1069 (1953).
2. A. Gover and Z. Livni, "Operation regimes of Cerenkov-Smith-Purcell free electron lasers and T.W. amplifiers," Opt. Commun. **26**, 375–380 (1978).
3. A. Gover and P. Sprangle, "A unified theory of magnetic bremsstrahlung, electrostatic bremsstrahlung, Compton-Raman scattering, and Cerenkov-Smith-Purcell free-electron lasers," IEEE J. Quantum Electron. **17**, 1196–1215 (1981).
4. L. Schächter and A. Ron, "Smith-Purcell free-electron laser," Phys. Rev. A **40**, 876–896 (1989).
5. J. Urata, M. Goldstein, M. Kimmitt, a. Naumov, C. Platt, and J. Walsh, "Superradiant Smith-Purcell Emission," Phys. Rev. Lett. **80**, 516–519 (1998).
6. S. E. Korbly, A. S. Kesar, J. R. Sirigiri, and R. J. Temkin, "Observation of frequency-locked coherent terahertz smith-purcell radiation," Phys. Rev. Lett. **94**, 1–4 (2005).
7. M. J. Moran, "X-ray generation by the Smith-Purcell effect," Phys. Rev. Lett. **69**, 2523–2526 (1992).
8. P. M. Van den Berg, "Smith-Purcell radiation from a point charge moving parallel to a reflection grating," J. Opt. Soc. Am. **63**, 1588–1597 (1973).
9. J. Brownell, J. Walsh, and G. Doucas, "Spontaneous Smith-Purcell radiation described through induced surface currents," Phys. Rev. E **57**, 1075–1080 (1998).
10. A. P. Potylitsyn, "Resonant diffraction radiation and Smith-Purcell effect," Phys. Lett. A **238**, 112–116 (1998).
11. A. Gover, P. Dvorkis, and U. Elisha, "Angular radiation pattern of Smith-Purcell radiation," J. Opt. Soc. Am. B **1**, 723 (1984).
12. L. Schächter and A. Ron, "Smith-Purcell free-electron laser," Phys. Rev. A **40**, 876–896 (1989).
13. S. L. Chuang and J. A. Kong, "Enhancement of Smith–Purcell radiation from a grating with surface-plasmon excitation," J. Opt. Soc. Am. A **1**, 672 (1984).
14. S. J. Glass and H. Mendlowitz, "Quantum theory of the Smith-Purcell experiment," Phys. Rev. **174**, 57–61 (1968).
15. S. Tsesses, G. Bartal, and I. Kaminer, "Light generation via quantum interaction of electrons with periodic nanostructures," Phys. Rev. A **95**, 13832 (2017).
16. J. R. M. Saavedra, D. Castells-Graells, and F. J. Garcia De Abajo, "Smith-Purcell radiation emission in aperiodic arrays," Phys. Rev. B - Condens. Matter Mater. Phys. **94**, 1–5 (2016).
17. I. Kaminer, S. E. Kooi, R. Shiloh, B. Zhen, Y. Shen, J. J. López, R. Remez, S. A. Skirlo, Y. Yang, J. D. Joannopoulos, A. Arie, and M. Soljačić, "Spectrally and Spatially Resolved Smith-Purcell Radiation in Plasmonic Crystals with Short-Range Disorder," Phys. Rev. X **7**, 11003 (2017).
18. Z. Wang, K. Yao, M. Chen, H. Chen, and Y. Liu, "Manipulating Smith-Purcell Emission with Babinet Metasurfaces," Phys. Rev. Lett. **117**, 157401 (2016).
19. See supplemental material for this Paper
20. G. Dattoli, A. Doria, G. P. Gallerano, L. Giannessi, K. Hesch, H. O. Moser, P. L. Ottaviani, E. Pellegrin, R. Rossmanith, R. Steininger, V. Saile, and J. Wüst, "Extreme ultraviolet (EUV) sources for lithography based on synchrotron radiation," Nucl. Instruments Methods Phys. Res. Sect. A Accel. Spectrometers, Detect. Assoc. Equip. **474**, 259–272 (2001).

21. M. Holler, M. Guizar-Sicairos, E. H. R. Tsai, R. Dinapoli, E. Müller, O. Bunk, J. Raabe, and G. Aeppli, "High-resolution non-destructive three-dimensional imaging of integrated circuits," Nature **543**, 402–406 (2017).

22. A. Ghisaidoobe and S. Chung, "Intrinsic Tryptophan Fluorescence in the Detection and Analysis of Proteins: A Focus on Förster Resonance Energy Transfer Techniques," Int. J. Mol. Sci. **15**, 22518–22538 (2014).

23. F. J. García de Abajo, "Interaction of Radiation and Fast Electrons with Clusters of Dielectrics: A Multiple Scattering Approach," Phys. Rev. Lett. **82**, 2776–2779 (1999).

24. Y. Yang, A. Massuda, C. Roques-Carmes, S. E. Kooi, T. Christensen, S. G. Johnson, J. D. Joannopoulos, O. D. Miller, I. Kaminer, and M. Soljačić, "Maximal Photon Emission and Energy Loss from Free Electrons," Submitted (n.d.).

25. Y.-C. Lai, T. C. Kuang, B. H. Cheng, Y.-C. Lan, and D. P. Tsai, "Generation of convergent light beams by using surface plasmon locked Smith-Purcell radiation," Sci. Rep. **7**, 11096 (2017).

26. F. Aieta, M. A. Kats, P. Genevet, and F. Capasso, "Multiwavelength achromatic metasurfaces by dispersive phase compensation," Science (80-.). **347**, 1342 (2015).

27. M. Berry, "Faster than Fourier," in *Quantum Coherence and Reality, Celebration of the 60th Birthday of Yakir Aharonov*, J. S. Anandan and J. L. Safko, eds. (World Scientific, 1994), pp. 55–65.

28. R. Remez and A. Arie, "Super-narrow frequency conversion," Optica **2**, 472–475 (2015).

29. W. H. Lee, "Binary computer-generated holograms.," Appl. Opt. **18**, 3661–3669 (1979).

30. G. Li, B. P. Clarke, J.-K. So, K. F. MacDonald, and N. I. Zheludev, "Holographic free-electron light source," Nat. Commun. **7**, 13705 (2016).